DOI: 10.13009/EUCASS2017-372

DOI: ADD DOINUMBER HERE

Accounting for wall roughness effects in turbulence models : a wall function approach

François Chedevergne⋆† *and Bertrand Aupoix*⋆
⋆*ONERA The French Aerospace Lab*
2 avenue Edouard Belin 31055 Toulouse Cedex 4
francois.chedevergne@onera.fr
†Corresponding author

Abstract

To meet expectations of simulation tools for ice accretion, requiring low CPU consuming flow solvers, a wall function has been developed to complement a RANS turbulent model involving roughness corrections.[1,2] The latter belongs to the classical family of equivalent sand grain models. The proposed wall model relies on the Suga *et al.* wall function approach.[21] Among the improvements brought by the new model, the wetted surface is now considered as a parameter that controls the heat transfer on rough walls. Validations test cases are discussed at the end of the paper, illustrating the improvements realized by the present model.

1. Introduction

Although most turbulence models concentrate on smooth walls, it is obviously essential to be able to account for roughness in some applications. For ice accretion on the leading edge of airfoils, modifications of heat transfers due to roughness is a key parameter. It is crucial to dispose of models capable of reproducing roughness effects on near wall flows to produce satisfactory predictions with icing codes. Other applications, such as in turbomachinery[7] , also faces similar difficulties for performance predictions. For instance, performance degradation assessment due to wear of the blades (deposit, erosion, pitting, ...) in turbines requires to account for surface roughness. Re-entry vehicles using ablative materials also present rough surfaces and for those vehicles the evaluation of heat transfer is a key design parameter.

The heat transfer and friction increases due to roughness result from different processes. In the full rough regime, the friction increase is due to pressure forces on roughness elements. Indeed, it is a drag increase. Concerning heat transfer increase, two separate origins can be highlighted. First the increase of the wetted surface due to roughness shapes contribute to the rise. In parallel, the turbulence agitation due to roughness leads to high heat diffusion. Consequently, compared to smooth surfaces, it is observed that rough walls produce higher drag increase than heat transfer increase. The Reynolds analogy that relates friction coefficients to Stanton numbers no longer holds for rough surfaces.

To reproduce these effects in numerical simulations, several approaches can be considered. First, flows around roughness can be directly computed without roughness models. So far these approaches are limited to a research level, Direct Numerical Simulations or Large Eddy Simulations resulting in unaffordable CPU costs for practical applications. Although less CPU ressources consuming, Reynolds Averaged Navier-Stokes computations are sometimes employed in conjunction with mesh resolved roughness but suffer from several weaknesses related to inherent RANS capabilities. The second approach refers to the Discrete Element Method.[18–20] Navier-Stokes equations are spatially averaged modifying the equations set to account for blockage effects of the roughness and also drag and heat transfer over the roughness elements. This promising method has been successfully applied in boundary layer codes. However, so far, the necessary equation modifications prevent its use in a RANS context and limits its scope. Finally, the most commonly adopted approach is the equivalent sand grain approach that rely on Nikuradse's experiments.[13,14] A two step process is used. The surface is characterized using correlations (or numerical process) to define the equivalent sand grain height h_s that would have led to the same roughness effects in Nikuradse's experiments. Then, h_s is used as a new parameter to alter turbulence models and reproduce roughness effects on flows.

Copyright © 2017 by François Chedevergne. Published by the EUCASS association with permission.

DOI: 10.13009/EUCASS2017-372

Recently, Aupoix[2] developed a roughness correction applied to the $k-\omega$ SST model. This correction allows to reproduce the drag increase at the wall due to roughness from the knowledge of the h_s parameter. Later on, a second correction was developed by Aupoix[1] to account for heat exchanges modifications due to roughness. Excellent agreement were obtained on a variety of boundary layer flows. As a standard turbulence model, it requires fine meshes at walls with y^+ values around unity or below. For ice accretion numerical tools, that requires many computational cycles involving a flow solver, it is of crucial importance to reduce at its maximum the CPU time per solver. Several approaches can be pursued such as a coupling between a Euler solver and an integral boundary layer code or wall functions adapted to Navier-Stokes formulations. In the present context, there is thus a true need to complete the current roughness corrections of Aupoix by developing a complementary wall function. The objective is to lower the mesh size used in the flow solver and thus to limit the CPU ressources. The paper presents the development of such a wall function approach. In the first part of the paper, principles that rules the corrections developed by Aupoix[1,2] are reminded. In a second part, the original analytical wall function approach of Suga *et al.*,[21] and from which the new model is build, will be exposed. Then, the formulation used in the present wall function will be detailed and a first validation on several boundary layer flows will be presented in order to highlight the progress made compared to the original formulation of Suga *et al.*[21]

2. Roughness corrections principles

In all the following, only distributed roughness will be considered, *i.e.* for which characteristic lengths (height, span and spacing) are small compared to boundary layer thickness. In addition, only k-type roughness,[15] for which effects are linked to their heights will be treated here.

2.1 Dynamic correction

Nikuradse[13,14] pointed out that above roughness the logarithmic law is preserved but shifted. The shift Δu^+ can be related to the equivalent sand grain height h_s and is given by Nikuradse from relations:

$$u^+ = \frac{1}{\kappa}\ln y^+ + C - \Delta u^+ \qquad u^+ = \frac{u}{u_\tau} \quad y^+ = \frac{y u_\tau}{\nu} \quad C = 5.5 \qquad \kappa = 0.40 \tag{1}$$

where the velocity profile u^+ is linked to h_s^+ through:

$$u^+ = \frac{1}{\kappa}\ln\frac{y^+}{h_s^+} + B \tag{2}$$

where

$$\begin{array}{rll} 1 < h_s^+ < 3.5 & B = 5.5 + \dfrac{1}{\kappa}\ln h_s^+ \\ 3.5 < h_s^+ < 7 & B = 6.59 + 1.52\ln h_s^+ \\ 7 < h_s^+ < 14 & B = 9.58 \\ 14 < h_s^+ < 68 & B = 11.5 - 0.7\ln h_s^+ \\ 68 < h_s^+ & B = 8.48 \end{array} \tag{3}$$

The shiflt Δu^+ can also be expressed in a more compact form provided by Grigson as:

$$\Delta u^+ = \frac{1}{\kappa}\ln\left(1 + \frac{h_s^+}{\exp(3.25\kappa)}\right) \qquad \kappa = 0.41 \tag{4}$$

The later expression is obtained from Colebrook's data.
Starting from this observation on boundary layer profiles, Aupoix and Spalart[3] proposed a strategy to reproduce this shift in turbulence models while artificially increasing turbulent viscosity μ_t at the wall. The leading principles are the following. A wall shift y_0 is introduced so that velocity gradients over rough and smooth surfaces reads:

$$\left.\frac{\partial u_r^+}{\partial y^+}\right|_{y^+} = \left.\frac{\partial u_l^+}{\partial y^+}\right|_{y^+ + y_0^+} \tag{5}$$

with subscripts r and s refers respectively to rough and smooth surfaces. Thus, one obtains after integrating the previous relation:

DOI: 10.13009/EUCASS2017-372

$$u_r^+(y^+) = u_l^+(y^+ + y_0^+) - u_l^+(y_0^+) \tag{6}$$

and then the shift Δu^+ is directly given by:

$$\Delta u^+ = u_l^+(y_0^+) \tag{7}$$

In boundary layer, considering a constant total shear, the momentum equation reduces to:

$$(1 + \mu_t^+)\frac{\partial u^+}{\partial y^+} = 1 \tag{8}$$

Finally, from eq. (5) one obtains:

$$\mu_{t_r}^+(y^+) = \mu_{t_l}^+(y^+ + y_0^+) \tag{9}$$

The initial search for a shift Δu^+ has been transferred to the search for a shift y_0^+ involving an eddy viscosity increase. In particular at the wall:

$$\mu_{t_{r_w}}^+ = \mu_{t_l}^+(y_0^+) \tag{10}$$

Practically, knowing a relation between Δu^+ and h_s^+ such as eq. (4), a smooth profile expression can be used to find y_0^+ satisfying eq. (7). Then, considering $k-\omega$ turbulence model, it is pretty easy to get $k_l^+(y_0^+)$ and $\omega_l^+(y_0^+)$ that provide k_w^+ and ω_w^+ values to be imposed at the wall to recover eq. (10). Expressions $k_w^+(h_s^+)$ and $\omega_w^+(h_s^+)$ have been obtained by Aupoix[2] and read:

$$\begin{aligned} k_w^+ &= \max\left(0; \frac{1}{\sqrt{\beta^*}}\tanh\left[\left(\frac{\ln\frac{h_s^+}{30}}{\ln 10} + 1 - \tanh\frac{h_s^+}{125}\right)\tanh\left(\frac{h_s^+}{125}\right)\right]\right) \\ \omega_w^+ &= \frac{300}{h_s^{+2}}\left(\tanh\frac{15}{4h_s}\right)^{-1} + \frac{191}{h_s^+}\left[1 - \exp\left(-\frac{h_s^+}{250}\right)\right] \end{aligned} \tag{11}$$

Note that relations of eq. (11) have been established using Colebrook's data and eq. (4). Equivalent relations have been obtained from Nikuradse's data by Aupoix.[2]

2.2 Thermal correction

As mentioned previously, the dynamic correction is an ad hoc correction that reproduce the pressure effect on drag through an increase of the eddy viscosity at the wall. In addition, since the Reynolds analogy no longer holds for rough surfaces, it is necessary to derive a thermal correction to account for heat transfer modifications. A simple way to derive such a correction is to modify the turbulent Prandtl number by wrtting:

$$Pr_t = Pr_{t_\infty} + \Delta Pr_t \tag{12}$$

where Pr_{t_∞} is the standard turbulent Prandtl number value 0.9. Increasing Pr_t decreases the turbulent conductivity and hence the heat transfer towards the wall and the heat flux. This limits the undesirable effect of the increase of the eddy viscosity. Several parameters rules the correction developed by Aupoix? to represent different physical behaviors. The thermal correction ΔPr_t must be restricted to a certain extent from the wall. An exponential decay involving the mean roughness height h has been introduced to this end. To account for turbulence diffusion and wetted surface effects, both h_s and S_{corr} parameters are used in the correction. The later is the corrected wetted surface ratio defined using the surface geometry where troughs below the reference (melt-down surface) are neglected. The final correction of Aupoix reads as follow:

$$\begin{aligned} \Delta Pr_t &= \mathcal{F} e^{-y/h} \\ \mathcal{F} &= A\Delta u^{+^2} + B\Delta u^+ \\ A &= (0,0155 - 0,0035 S_{corr})\left(1 - \exp(-12(S_{corr} - 1))\right) \\ B &= -0,08 + 0,25\exp(-10(S_{corr} - 1)) \\ \Delta u^+ &= \Delta u^+(h_s^+) \end{aligned} \tag{13}$$

DOI: 10.13009/EUCASS2017-372

Both dynamic and thermal corrections have been extensively validated[1,2] in a boundary layer context using ONERA's code CLICET. Recently they have been introduced in Navier-Stokes solvers for testing.

3. Analytical wall function principles

Following ideas of Craft *et al.*,[8] Suga *et al.*[21] developed an extension of the Analytical Wall Function (AWF) to account for wall roughness. This wall model has been originally developed for structured codes. The main idea of the AWF is to impose a linear evolution to the eddy viscosity in the internal region of the boundary layer. The logarithmic behaviour is not directly imposed to the velocity profile but results from the linearity of μ_t. The idea comes from the following relation:

$$\mu_t = \rho C_\nu \sqrt{k} l = \rho C_\nu \sqrt{k} \kappa y \approx \alpha \mu y^* \tag{14}$$

where $y^* = \dfrac{y\sqrt{k_P}}{\nu}$ is a characteristic Reynolds number for wall cells which center is denoted P. Constant $C_\nu = C_\mu^{1/4}$ with $C_\mu = 0.09$. In order to have a viscous sublayer where $\mu_t \ll \mu$, a distance y_v is introduced such that:

$$\mu_t = \max\left(0, \alpha\mu(y^* - y_v^*)\right) \tag{15}$$

with constant $\alpha = \kappa C_\nu$. Bidimensional boundary layer equations reduce to:

$$\begin{aligned} \frac{\partial}{\partial y^*}\left[(\mu+\mu_t)\frac{\partial u}{\partial y^*}\right] &= \frac{\nu^2}{k_P}\left[\frac{\partial}{\partial x}(\rho u u) + \frac{\partial P}{\partial x}\right] = C_u \\ \frac{\partial}{\partial y^*}\left[\left(\frac{\mu}{Pr} + \frac{\mu}{Pr_t}\right)\frac{\partial T}{\partial y^*}\right] &= \frac{\nu^2}{k_P}\left[\frac{\partial}{\partial x}(\rho u T) + S_T\right] = C_T \end{aligned} \tag{16}$$

with S_T the averaged energy source term over the cell P. Considering C_u and C_T as constants, and using eq. (15) for μ_t, analytical expressions for velocity and temperature profiles can be easily reached. Since we have:

$$\begin{aligned} \frac{\mathrm{d}u}{\mathrm{d}y^*} &= \frac{C_u y^* + A_u}{\mu + \mu_t} \\ \frac{\mathrm{d}T}{\mathrm{d}y^*} &= \frac{C_T y^* + A_T}{\dfrac{\mu}{Pr} + \dfrac{\mu_t}{Pr_t}} \end{aligned} \tag{17}$$

wall friction τ_w and heat transfer ϕ_w have analytical expressions:

$$\begin{aligned} \tau_w &= \frac{\sqrt{k_P} A_u}{\nu} \\ \phi_w &= -\frac{\rho C_p \sqrt{k_P} A_T}{\mu} \end{aligned} \tag{18}$$

Associated with these models for friction and heat transfer at the wall, production and dissipation terms for the turbulent kinetic energy are modeled:

$$P_k = \begin{cases} 0 & \text{for } y^* < y_v^* \\ \nu_t\left(\dfrac{\mathrm{d}u}{\mathrm{d}y}\right)^2 = \dfrac{\alpha k_P}{\nu}(y^* - y_v^*)\left(\dfrac{C_u y^* + A_u}{\mu + \mu_t}\right)^2 & \text{for } y^* \geq y_v^* \end{cases} \tag{19}$$

and

$$\varepsilon = \begin{cases} \dfrac{2\nu k_P}{y_\varepsilon^2} & \text{for } y < y_\varepsilon \\ \dfrac{k_P^{3/2}}{c_l y} & \text{for } y \geq y_\varepsilon \end{cases} \tag{20}$$

where a dissipation scale y_ε is defined through $y_\varepsilon^* = 2c_l$, with $c_l = 2.55$. Mean values are computed through integration over the cell. Let N designate the distance to the wall of the upper face of the wall cell. Integration over $[0, y_N]$ is straightforward for $\overline{P_k}$ and reads for $\overline{\varepsilon}$:

DOI: 10.13009/EUCASS2017-372

$$\overline{\varepsilon} = \begin{cases} \dfrac{2k_P^2}{\nu y_\varepsilon^{*2}} & \text{for } y_N^* < y_\varepsilon^* \\ \dfrac{k_P^2}{\nu y_N^*}\left(\dfrac{2}{y_\varepsilon^*} + \dfrac{1}{c_l}\ln\left(\dfrac{y_N^*}{y_\varepsilon^*}\right)\right) & \text{for } y_N^* \geq y_\varepsilon^* \end{cases} \tag{21}$$

In the original model of Craft *et al.*[8] a numerical optimization on smooth flat plate configurations has led to impose $y_v^* = 10.7$.
To reproduce the logarithmic law shift Δu^+ due to roughness, Suga *et al.* authorized y_v^* to vary with respect to equivalent sand grain height h_s. For increasing values of h_s, y_v must decrease to induce an increase of μ_t at the wall and thus increase the friction. The modified model for rough wall is:

$$y_{v_r}^* = y_v^*\left(1 - \left(\frac{h_s^*}{70}\right)^m\right) \qquad m = \max\left(\left(0,5 - 0,4\left(\frac{h_s^*}{70}\right)^{0,7}\right), \left(1 - 0,79\left(\frac{h_s^*}{70}\right)^{-0,28}\right)\right) \tag{22}$$

For the thermal effect, Suga *et al.* proposes a similar formulation to Aupoix's, see eq. (13):

$$\Delta Pr_t = \mathcal{F}\max\left(0, 1 - \frac{y^*}{h_s^*}\right) \qquad \mathcal{F} = \frac{5,5}{1 + \left(\dfrac{h_s^*}{70}\right)^{6,5}} + 0,6 \tag{23}$$

However, at a first glance, eq. (23) looks surprising since it only depends on h_s and $\Delta Pr_t \to 0.6$ at the wall for $h_s^* \to +\infty$.

4. Wall function formulation

Going back over the idea of introducing a wall shift y_0 according to eq. (7), a new model for y_v has been build. In order to get a general expression for y_0, the Reichardt's law for a smooth zero pressure gradient flat plate velocity profile is considered:

$$u^+ = \frac{1}{\kappa} ln\left(1 + \kappa y^+\right) + 7.8\left(1 - \exp(-\frac{y^+}{11}) - \left(\frac{y^+}{11}\right)\exp(-0.33y^+)\right) \tag{24}$$

From this profile, the shift y_0^+ is computed with respect to h_s^+. Fitting functions are determined for both Δu^+ variants, see eq. (2) and eq. (4). They read:

$$\begin{aligned} y_0^+ &= \max\left(0; 3,25\ln\left(h_s^{+0,9}\right) - 5,5\right)\exp\left(-\frac{h_s^+}{880}\right) + 0,0318h_s^+ && \text{using Nikuradse's data} \\ y_0^+ &= (0.0202h_s^+ + 10.1)\tanh\left(\left(\frac{h_s^+}{90}\right)^{0.55}\right) && \text{using Colebrook's data} \end{aligned} \tag{25}$$

Figure 1 show the behaviors of the shift y_0^+. A difference in the slope in the full rough regime can be observed. It comes from the influence of the Karman constant κ on the Δu^+ evolution already evidenced by Aupoix.[2]

Since in the inner region of the boundary layer $\mu_t^+ = \left(\dfrac{\partial u^+}{\partial y^+}\right)^{-1} - 1$, Reichardt's profile directly provides $\mu_t^+(y_0^+)$ which corresponds to $\mu_{t_w}^+(h_s^+)$. Finally, as $y_{v_r}^* = -\dfrac{\mu_{t_w}^+}{\alpha}$, a fitting function is calculated and yields:

$$\begin{aligned} y_{v_r}^* &= \frac{1}{\alpha}\left(\frac{h_s}{165}\right)^{1,3}\left[2\exp\left(-\left(\frac{h_s^+}{100}\right)^{0,9}\right) + 1\right]\left[\left(\left(\frac{h_s^{+0.8} - 11}{8}\right)^2 - 2,5\right)\exp\left(-\left(\frac{h_s^+}{20}\right)^{1,2}\right) + 1\right] \\ &\quad + y_v^*\exp(-2h_s^+) \quad \text{using Nikuradse's data} \\ y_{v_r}^* &= -\frac{1}{\alpha}\left(\frac{k_s^+}{180}\right)^{1,15}\left[1 + 2\exp\left(-\left(\frac{k_s^+}{100}\right)^{0,9}\right)\right]\left[1 - 0,4\exp\left(-\left(\frac{k_s^+}{100}\right)^{1,2}\right)\right]\left(1 + \ln\left(k_s^{+-0,9}\right)\right)\exp\left(-\frac{k_s^+}{7}\right) \\ &\quad + y_v^*\exp(-2k_s^+) \quad \text{using Colebrook's data} \end{aligned} \tag{26}$$

DOI: 10.13009/EUCASS2017-372

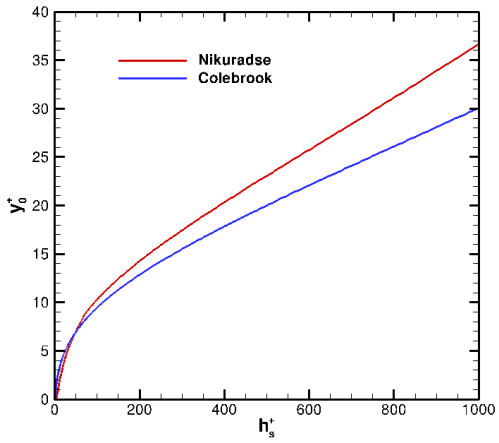

Figure 1: Wall shifts y_0^+ obtained from Nikuradse's data and for Colebrook's data

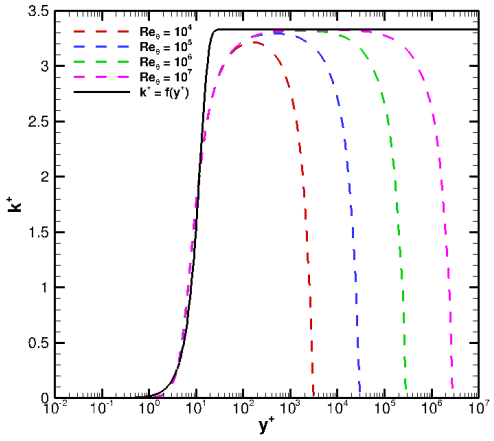

Figure 2: Turbulent kinetic energy profiles k^+ of zero pressure gradient flat plate boundary layers

Note that the last term serves as a recovery term for smooth configurations.

The Reynolds number introduced by Craft *et al.* y^* is directly linked to the standard nondimensional distance y^+ through:

$$y^* = \frac{y\sqrt{k_P}}{\nu} = \frac{yu_\tau}{\nu}\frac{\sqrt{k}}{u_\tau} = y^+\sqrt{k^+} \tag{27}$$

Bradshaw's relation gives:

$$y^* = \frac{y^+}{\sqrt{a_1}} \qquad k^+ = \frac{1}{a_1} \qquad a_1 = 0.3 \tag{28}$$

but is restricted to the logarithmic region. To account for the whole inner region, the k^+ profile obtained with the $k-\omega$ SST model has been modeled as:

$$k^+ = \frac{1}{a_1}\tanh\left(0,005y^{+2}\right) \tag{29}$$

On figure 2 several turbulent kinetic energy profiles have been plotted. They have been obtained with the CLICET code for the $k-\omega$ SST model and correspond to solutions at various R_θ values, R_θ being the Reynolds number based

DOI: 10.13009/EUCASS2017-372

upon the momentum. Relation (29) is a rather good approximation in the inner region of boundary layers.
Finally, figures 3(a) and 3(b) compare evolution of μ_{t_w} obtained with Suga *et al.* model and for both variants of the present model. Important differences are visible on those figures. For low h_s^+ values, *i.e.* below 70, the model proposed

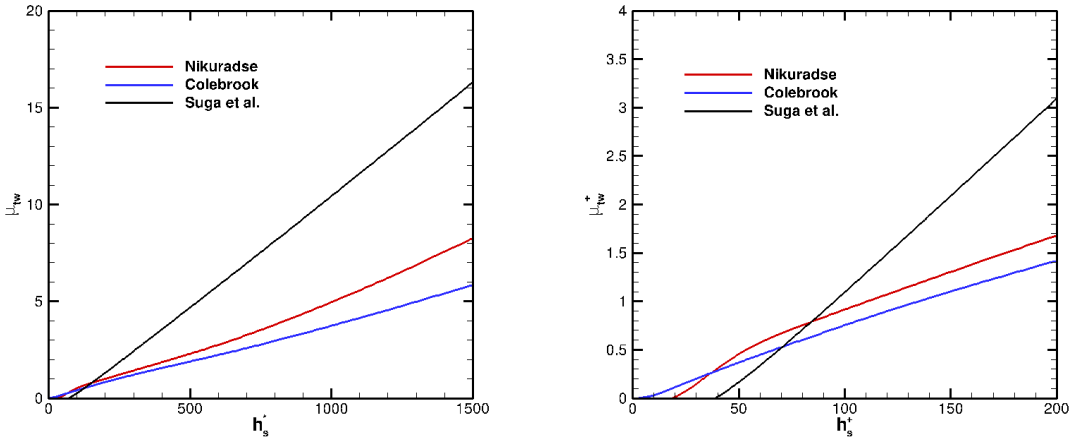

(a) $\mu_{t_w} = f(h_s^*)$ (b) $\mu_{t_w} = f(h_s^+)$

Figure 3: Eddy viscosity at the wall with respect to nondimensional equivalent sand grain heights

by Suga *et al.* exhibit lower values whereas for larger h_s^+ values it reaches much higher values compared to μ_{t_w} values obtained from eq. (26). The limit value $h_s^+ = 70$ corresponds incidentally to the entrance into the full rough regime without any obvious reason for that.

Due to the introduction of wall shift y_0^+, a modification of the averaged production term $\overline{P_k}$ and of the averaged dissipation rate $\overline{\varepsilon}$ is made. For $\overline{P_k}$ the lower limit of integration must be shifted, see appendix, whereas for the dissipation rate $\overline{\varepsilon}$ one writes:

$$\overline{\varepsilon} = \begin{cases} \dfrac{2k_P^2}{\nu y_\varepsilon^{*2}} & \text{if } y_N^* < y_\varepsilon^* \\ \dfrac{k_P^2}{\nu\left(y_N^* - y_0^*\right)}\left(\dfrac{2\left(y_\varepsilon^* - y_0^*\right)}{y_\varepsilon^*} + \dfrac{1}{c_l}\ln\left(\dfrac{y_N^*}{y_\varepsilon^*}\right)\right) & \text{if } y_N^* \geq y_\varepsilon^* \geq y_0^* \\ \dfrac{k_P^2}{\nu\left(y_N^* - y_0^*\right)c_l}\ln\left(\dfrac{y_N^*}{y_0^*}\right) & \text{if } y_n^* \geq y_0^* \geq y_\varepsilon^* \end{cases} \tag{30}$$

Concerning the thermal correction, work by Suga *et al.* is leveraged using modified Prandtl number given by eq. (13). However, in order to ease integral calculations, the exponential behavior is altered as follows:

$$\Delta Pr_t = \mathcal{F}\max\left(0, 1 - \frac{y^*}{a h_s^*}\right) \tag{31}$$

with $a = h/h_s$. Details on the impact of a on the computation of heat transfer are given in the appendix.

To illustrate and evidence differences that exist between Suga *et al.* thermal correction and the proposed Prandtl number modification, correction $\Delta Pr_t|_{y=0} = \Delta Pr_{t_w}$ at the wall are depicted on figure 4. To highlight the influence of the corrected wetted surface ratio S_{corr} three curves are plotted on figure 4 for the present model. Although large discrepancies exist for low values of h_s^+, the Suga *et al.* model should be analyzed carefully in this range. Indeed, for $h_s^* < 70$ the model provides $y_{v_r} > 0$ involving $\mu_{t_w} = 0$. Thus, the turbulent thermal conductivity λ_t will be zero at the wall regardless the value of the turbulent Prandtl number Pr_t. Nevertheless, beyond the effect of S_{corr}, for large values of h_s^+ major differences appear in the behavior of ΔPr_{t_w} between Suga et al. model and the present one.

DOI: 10.13009/EUCASS2017-372

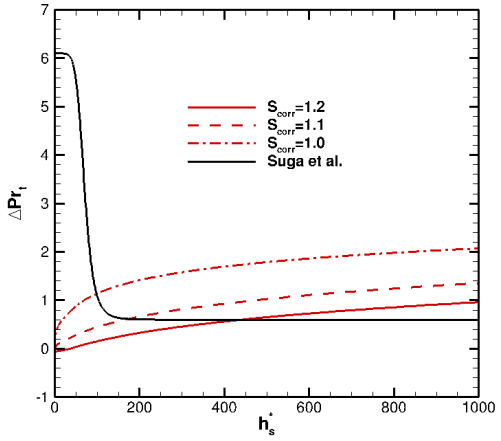

Figure 4: Thermal correction ΔPr_{t_w} at the wall

5. First validation

The final objective of this work is to amend the $k-\omega$ SST model including roughness corrections[1,2] so that it can be used with coarse meshes near walls. But before introducing the model into a Navier-Stokes solver, the wall function has been tested in the boundary layer code CLICET. The code has been slightly modified to permit the implementation of both Suga *et al.* model and the two variants presented above. Among options for implementing such wall functions in a boundary layer code, those compatible with unstructured Navier-Stokes solvers requirements have been made our first choices. The mesh self-adapts automatically in order that the user can prescribe the y_1^+ value of the first mesh point. Note that $y_1 = y_N$.
First, smooth configurations have been tested with the Craft *et al.* model[8] in order to validate the code modifications. In the following, two flat plate experiments will be examined. To begin with, experiments conducted by Blanchard[6] are used to analyze the behavior of the wall function approach on friction regardless of thermal effects. In the second experiments by Hosni it et al.,[9–11] a focus will be made on thermal effects due to roughness. In particular, the effect of the wetted surface on heat transfers will be emphasized.
Computations based upon Suga *et al.* model use standard $k-\omega$ SST turbulence model whereas the corresponding roughness corrections are used for computations involving Nikuradse or Colebrook variant of the new wall function. This is in line with the development of all these models.

5.1 Blanchard's experiments

Blanchard's experiments are interesting because the effect of an adverse pressure gradient has been measured for rough flat plate. Despite a rather low pressure gradient in the experiments, a significant reduction of the friction coefficient $C_f/2 = \tau_w/(\rho U_\infty^2)$ can be observed. Two configurations, with and without pressure gradient, have already been tested by Aupoix[2] to validate his roughness corrections. For this reason, fine mesh computations, corresponding to a low-Reynolds number approach, have also been conducted and can serve as reference, in addition to measurements. The equivalent sand grain height is estimated to $h_s^+ \approx 150$ with $h = 0,425$ mm in the zero pressure gradient (ZPG) configuration. On figures 5(a) and 5(b) are plotted friction coefficients C_f along the plate for several computations. Two low-Re computations for both variants based on Nikuradse and Colebrook's data are shown. Three additional computations with wall functions activated and $y_1^+ = 200$ are also plotted. Results clearly prove the efficiency of the Suga *et al.* model and the present one to reproduce the effect of roughness on friction coefficients for ZPG and APG configurations. As shown in figure 3(b), for $h_s^+ < 200$ all models provide similar order of magnitude for μ_{t_w}, explaining the good behaviors observed in figures 5(a) and 5(b). Moreover, the use of wall functions also permit to account for adverse pressure gradient on rough surfaces.
To complete these results, a series of five complemetary computations for each of the wall functions have been conducted to evaluate the influence of y_1^+. On figure 6(a), 6(b) and 6(c) are plotted results for the ZPG case whereas on figures 7(a), 7(b) and 7(c) are shwon those for the APG configuration.

Several remarks can be made. First, generally speaking results are more dispersed on the ZPG case than on the

DOI: 10.13009/EUCASS2017-372

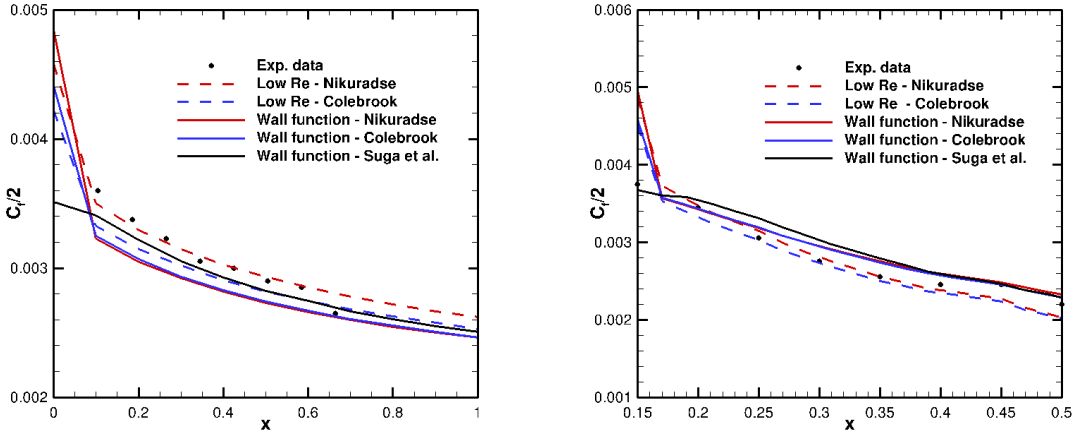

(a) ZPG (b) APG

Figure 5: Friction coefficients along the plate in Blanchard's experiments. Left, the zero pressure gradient case (ZPG). Right, the adverse pressure gradient case (APG).

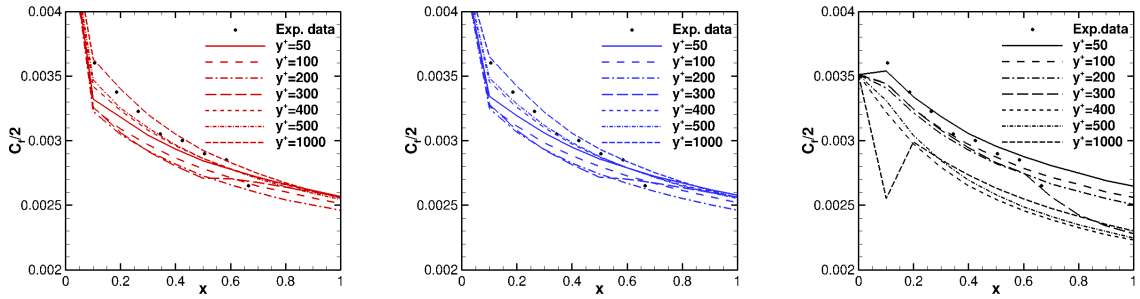

(a) Nikuradse (b) Colebrook (c) Suga *et al.*

Figure 6: Effect of y_1^+ on the friction coefficient in the ZPG case of Blanchard's experiments.

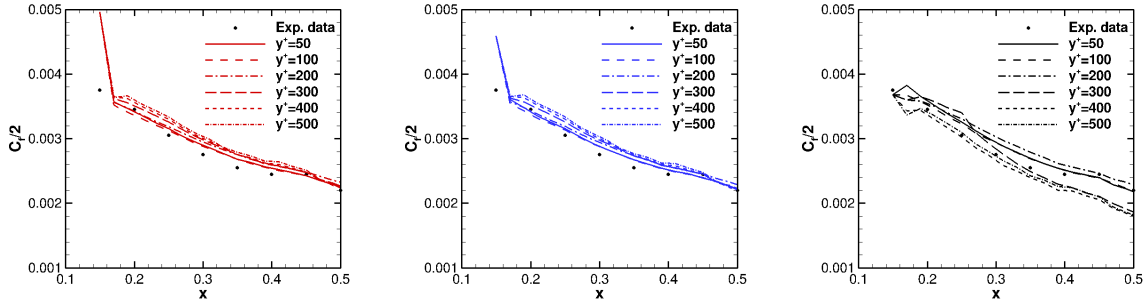

(a) Nikuradse (b) Colebrook (c) Suga *et al.*

Figure 7: Effect of y_1^+ on the friction coefficient in the APG case of Blanchard's experiments.

APG case. The pressure gradient introduce an additional constraint that limit dispersion. Second, the new wall function approach provide less dispersed results than Suga *et al* model. But, it is rather satisfactory to notice than for a wide range of y_1^+ values and distributed on both sides of h_s^+, results are quite in agreement with measurements. For very large

DOI: 10.13009/EUCASS2017-372

values of y_1^+ located above the logarithmic region, it is even surprising to have such reasonable results since some of the constitutive hypothesis no longer hold there.

5.2 Hosni *et al.* experiments

For these flat plate tests, surfaces are equipped with hemispheres having a diameter $D = 1.27$ mm and spaced in staggered rows with a spacing $L/D = 2$. Several freestream velocity U_∞ have been tested but in the present paper only $U_\infty = 58$ m/s is considered. Calculating S_{corr} is stragihtforward, one finds $S_{corr} = 1.17$.
This validation test case has already been considered by Suga *et al.* in their original paper.[21] However, these authors gives $h_s = 0.63$ mm and $h_s^+ = 120$ mm. From velocity profiles,[10] graphically one finds $\Delta u^+ = 11$ as illustrated on figure 9 for the location $x = 0.86$ m. Assuming a full rough regime, an estimate of the equivalent sand grain can be made from eq. (4) $h_s^+ = \exp(\kappa(\Delta u^+ + 2.98)) = 308$. Otherwise, according to the Waigh and Kind correlation[22] $h_s = 1.58$ mm and as for $x = 0.86$ Hosni *et al.*[10] gives $C_f = 0.05777$ leading thus to:

$$h_s^+ = \frac{h_s u_\tau}{\nu} = \frac{h_s}{\nu} U_\infty \sqrt{\frac{C_f}{2}} = 311 \tag{32}$$

This value is retained for computations in all the following. A low-Reynolds computation is performed using Colebrook's variant for roughness corrections. Three complementary computations are then realized for the different wall functions with $y_1^+ = 200$. Figure 8(a) and 8(b) show the obtained results for the friction coefficient C_f and for the Stanton number $St = -\phi_w/(\rho U_\infty C_p(T_w - T_\infty))$.

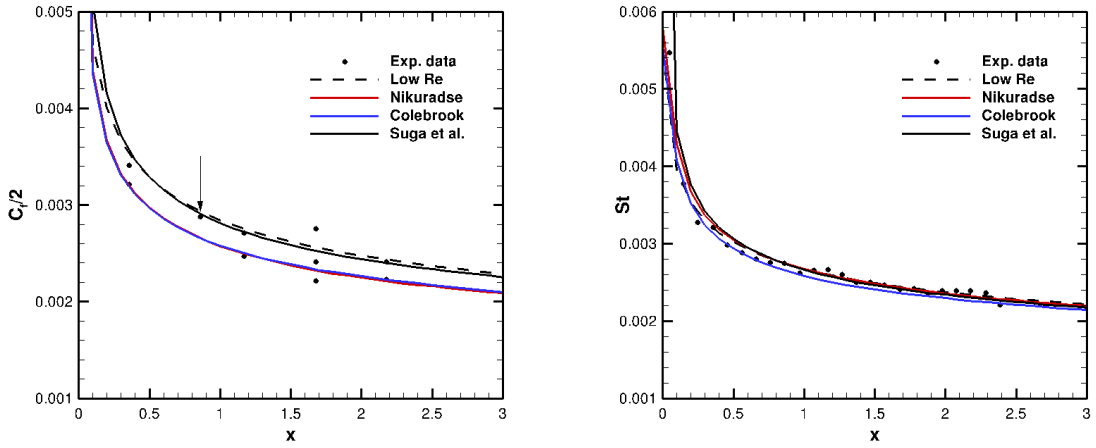

(a) friction coefficient

(b) Stanton number

Figure 8: Comparisons of friction coefficient and Stanton number for the flat plate equipped with hemispheres in Hosni *et al.* experiments. Results obtained using wall functions have been computed with $y_1^+ = 200$.

Given dispersion of the measurements points, it is hard to bring out one of the models. They all give good results. Effects of hemispheres are recovered for friction increase as well as for heat transfer increase.

Let's now consider one location on the plate $x = 0.86$ m. On figure 8(a), the arrow indicates that this location favors results obtained with a low-Re approach and the Suga *et al.* model for which u_τ is very close to the measured value. From hot wire measurements provided by Hosni *et al.*, the dimensionless velocity profile is plotted in a semi logarithmic diagram on figure 9. Experimental data are plotted with respect to y^+ and $y^+ - \Delta y^+$, Δy^+ being a wall shift linked to the existence of a roughness sublayer. Δy^+ has nothing to do with y_0^+ but is introduced to indicate that within the roughness and below a certain distance from the wall there is no fluid motion. Δy^+ is the fictitious origin of the wall distances. Jackson[12] proposes to define the Δy^+ shift as the point of application of the drag force on roughness elements. According to Jackson, Δy ranges from $0.5h$ to $0.84h$. Here, we consider $\Delta y = 0.7h = 0.4445$ mm namely $\Delta y^+ = 80$. With this shift, the measured velocity profile has an extended logarithmic zone.

DOI: 10.13009/EUCASS2017-372

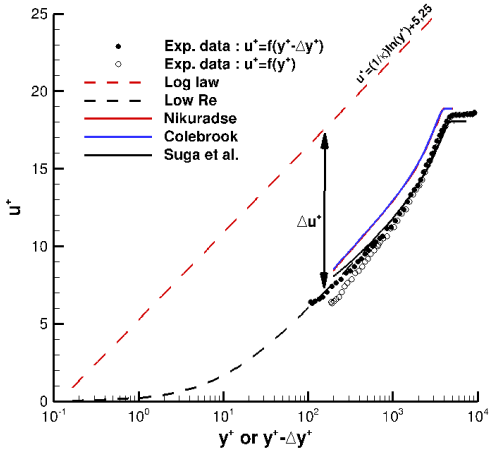

Figure 9: Velocity profiles plotted in wall variables for location $x = 0.86$ m on the fat plate equipped with hemispheres in Hosni *et al.* experiments.

Figure 9 highlights the value of Δu^+ and prove that velocity profiles are not altered by wall functions. Finally, a y_1^+ dependence study is realized. Due to numerical failures when using Suga *et al.* model, only results for the new model are available. Nevertheless, this does not mean that Suga *et al.* model is not as robust as the new model. In a Navier-Stokes solver, the model has been proved[21] to be efficient and robust.

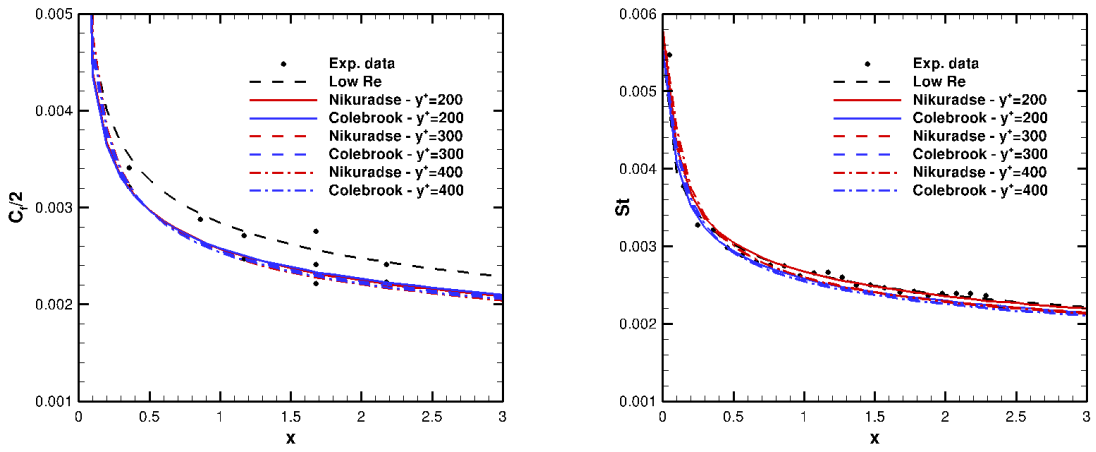

(a) friction coefficient

(b) Stanton number

Figure 10: Effect of y_1^+ on friction coefficient and Stanton number for the plate equipped with hemispheres in Hosni *et al.* experiments.

Due to a limited initial boundary layer thickness, y_1^+ values must remain below 400. Figure 10(a) and 10(b) confirm the good behavior of the new model when changing y_1.

What makes Hosni *et al.* experiments even more interesting is that they also performed measurements on flat plate equipped with truncated cones[9] that lead to the same dynamical effect as hemispheres do. Cones have a base diameter equals to that of the hemisphere, are truncated at $D/2$ and have a half top angle of 40^o. The spacing remains identical to the previous one. Thus, cones and hemispheres provide identical friction increase and may be represented using the same h_s value. But, Hosni *et al.*[9] prove that heat transfer are affected by the roughness shapes. The difference comes from the wetted surface that is lower for cones that for hemispheres. In the model, it results in a smaller value of S_{corr} for cones, being $S_{corr} = 1.09$.

DOI: 10.13009/EUCASS2017-372

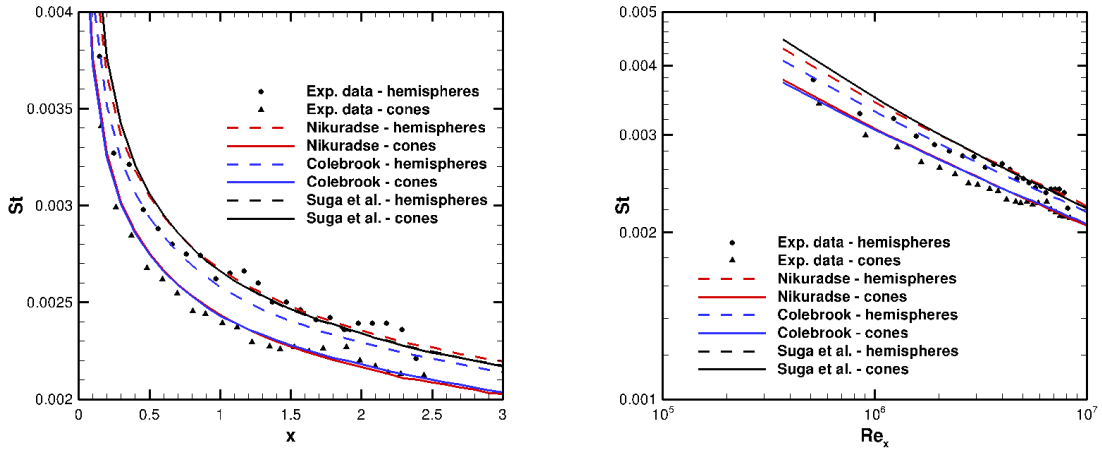

(a) linear scale (b) logarithmic scale

Figure 11: Influence of S_{corr} on heat transfer for two flat plate equipped with hemispheres and truncated cones respectively in Hosni *et al.* experiments.

Figures 11(a) and 11(b) clearly point out the modification of the Stanton number between the two configurations. The two variants of the wall function proposed in this paper permit to reproduce the observed effect, even if there is a slight underestimation. By construction, Suga *et al.* model is unable to capture this effect.

6. Conclusion and perspectives

A wall function, complementary to the roughness corrections developed by Aupoix,[1,2] has been developed relying on the approach initiated by Suga *et al.*[21] The resulting model has been sought to work in conjunction with the $k-\omega$ SST model including the roughness corrections. As for the corrections, two variants referring to Nikuradse or Colebrook's data have been build. One of the major improvement compared to the original work of Suga *et al.* is the dependence on the wetted surface through parameter S_{corr} of the turbulent Prandtl number. As a result, the new model is able to reproduce effects linked to roughness shapes on the heat transfers. This has been highlighted through comparisons of Stanton numbers obtained on configurations studied by Hosni *et al.*[9–11] at Mississippi State University. Moreover, the proposed wall function is found to be less depending on the altitude of the first point y_1^+ compared to Suga *et al.*. In practice, this means that the mesh dependence will be reduced. Indeed, the wall function is currently being implemented in the unstructured CEDRE code.[17] The main objective is then to compare this wall function approach in a RANS context to an approach combining a Euler solver coupled to an integral boundary layer code.[4,5] The most convincing approach in terms of CPU ressources, robustness and accuracy will be retained to be used as a flow solver in the icing simulation chain IGLOO3D[16] developed at ONERA.

7. Acknowledgments

The first author is very grateful to Bertrand Aupoix for sharing his knowledge and transmitting a remarkable collection of documents and data on rough walls.

8. Appendix

To identify the impact on coefficient a, see eq. (31), case $y_v^* < 0$ is detailed hereinafter. We start with:

$$\frac{\partial T}{\partial y^*} = \frac{Pr}{\mu}\frac{C_T y^* + A_T}{1 + \Theta_T\left(y - y_{v_r}^*\right)} \tag{33}$$

and :

DOI: 10.13009/EUCASS2017-372

$$\begin{aligned}\Theta_T &= \alpha\frac{Pr}{Pr_t} = \alpha\frac{Pr}{Pr_{t_\infty} + \mathcal{F}\left(1 - \dfrac{y^*}{ah_s^*}\right)} \quad \text{for} \quad y^* < h_s* \\ \Theta_T &= \alpha\frac{Pr}{Pr_{t_\infty}} \quad \text{for} \quad y^* \geq h_s^*\end{aligned} \tag{34}$$

After integration in the range $[y_0^*, h_s^*]$ one finds:

$$\begin{aligned}T_h - T_0 &= -\frac{Pr}{\mu}\frac{C_T\beta_T/a}{2(\alpha_T - \beta_T/a)}\left(h_s^{*^2} - y_0^{*^2}\right) - A_T\frac{Pr}{\mu}\frac{\beta_T/a}{\alpha_T - \beta_T/a}\left(h_s^* - y_0^*\right) \\ &+ \frac{PrC_T}{\mu\left(\alpha_T - \beta_T/a\right)^2}\left(\alpha_T H_s^{\beta_T,1} - \left(1 + \frac{1}{a}\right)\beta_T\lambda_b\right)\left(h_s^* - y_0^*\right) \\ &+ A_T\frac{Pr}{\mu}\left(\frac{\alpha_T H_s^{\beta_T,a}}{\left(\alpha_T - \beta_T/a\right)^2}\right)\ln\left[\frac{\Lambda_h^{\alpha\beta}}{\Lambda_0^{\alpha\beta}}\right] - \frac{Pr}{\mu}\frac{\lambda_b C_T}{\left(\alpha_T - \beta_T/a\right)^3}\left(\alpha_T H_s^{\beta_T,1} - \left(1 + \frac{1}{a}\right)\beta_T\lambda_b\right)\ln\left[\frac{\Lambda_h^{\alpha\beta}}{\Lambda_0^{\alpha\beta}}\right]\end{aligned} \tag{35}$$

whereas for $y^* \in [h_s^*, y_n^*]$ one gets:

$$T_n - T_h = \frac{Pr}{\mu}\frac{C_T}{\alpha_T}\left(y_n^* - h_s^*\right) + \frac{Pr}{\mu}\left(\frac{A_T}{\alpha_T} - \frac{C_T}{\alpha_T^2}Y_w^{\alpha_T}\right)\ln\left[\frac{Y_n^{\alpha_T}}{H_s^{\alpha_T}}\right] \tag{36}$$

with:

$$\begin{cases}\alpha_T = \alpha\dfrac{Pr}{Pr_{t_\infty}} \\ \beta_T = \dfrac{\mathcal{F}}{h_s^* Pr_{t_\infty}} \\ Y^{\alpha_T} = 1 + \alpha_T\left(y^* - y_v^*\right) \\ Y^{\beta_T,a} = 1 + \beta_T\left(y^* - y_v^*/a\right) \\ \lambda_b = Y_w^{\alpha_T} + \beta_T h_s^* \\ \Lambda^{\alpha\beta} = \lambda_b + y^*\left(\alpha_T - \beta_T/a\right)\end{cases} \tag{37}$$

Combining both expressions it is easy to get coefficients D_T and E_T such that $A_T = \dfrac{\dfrac{\mu}{Pr}\left(T_n - T_0\right) + C_T E_T}{D_T}$:

$$\begin{aligned}D_T &= \frac{1}{\alpha_T}\ln\left[\frac{Y_n^{\alpha_T}}{H_s^{\alpha_T}}\right] - \frac{\beta_T/a}{\alpha_T - \beta_T/a}\left(h_s^* - y_0^*\right) \\ &+ \frac{\alpha_T H_s^{\beta_T,a}}{\left(\alpha_T - \beta_T/a\right)^2}\ln\left[\frac{\Lambda_h^{\alpha\beta}}{\Lambda_0^{\alpha\beta}}\right] \\ E_T &= \frac{1}{\alpha_T}\left(h_s^* - y_n^*\right) + \frac{Y_w^{\alpha_T}}{\alpha_T^2}\ln\left[\frac{Y_n^{\alpha_T}}{H_s^{\alpha_T}}\right] + \frac{\beta_T/a}{2(\alpha_T - \beta_T/a)}\left(h_s^{*^2} - y_0^{*^2}\right) \\ &- \frac{1}{\left(\alpha_T - \beta_T/a\right)^2}\left(\alpha_T H_s^{\beta_T,1} - \left(1 + \frac{1}{a}\right)\beta_T\lambda_b\right)\left(h_s^* - y_0^*\right) \\ &+ \frac{\lambda_b}{\left(\alpha_T - \beta_T/a\right)^3}\left(\alpha_T H_s^{\beta_T,1} - \left(1 + \frac{1}{a}\right)\beta_T\lambda_b\right)\ln\left[\frac{\Lambda_h^{\alpha\beta}}{\Lambda_0^{\alpha\beta}}\right]\end{aligned} \tag{38}$$

Suga *et al*[21] only consider cases where $y_P \geq h_s$. In some configurations h_s can be very large and this limitation is too strict. The same is true for small values of h_s with very thin boundary layers. The model has been extended to cases $y_N \leq h_s$.

Note that the shift y_0 has only been considered for calculating $\overline{P_k}$. Minor modifications may be made to expressions given by Suga *et al.*[21] to account for y_0 in the calculation of A_u and A_T, as shown above.

DOI: 10.13009/EUCASS2017-372

References

[1] B. Aupoix. Improved heat transfer predictions on rough surfaces. *International Journal of Heat and Fluid Flows*, 56:160–171, December 2015.

[2] B. Aupoix. Roughness Corrections for the $k-\omega$ Shear Stress Transport Model: Status and Proposals. *Journal of Fluids Engineering*, 137:021202, February 2015.

[3] B. Aupoix and P.R. Spalart. Extensions of the Spalart–Allmaras turbulence model to account for wall roughness. *International Journal of Heat and Fluid Flows*, 24:454–462, 2003.

[4] C. Bayeux, E. Radenac, and P. Villedieu. Theory and validation of a 2d finite-volume integral boundary layer method intended for icing applications. In *47th AIAA Fluid Dynamics Conference*, number AIAA 2017-3976, Denver, Colorado, 2017. AIAA AVIATION Forum.

[5] N. Bempedelis, C. Bayeux, G. Blanchard, E. Radenac, and P. Villedieu. A 3d finite-volume integral boundary layer method for icing applications. In *9th AIAA Atmospheric and Space Environments Conference*, number AIAA 2017-3417, Denver, Colorado, 2017. AIAA AVIATION Forum.

[6] A. Blanchard. *Analyse Expérimentale et Théorique de la Structure de la Turbulence d'une Couche Limite sur Paroi Rugueuse*. PhD thesis, Université de Poitiers U.E.R.–E.N.S.M.A., 23 Juin 1977.

[7] J.P. Bons, R.P. Taylor, S.T. McClain, and R.B. Rivir. The many faces of turbine surface roughness. *Journal of Turbomachinery*, 123:739–748, October 2001.

[8] T.J. Craft, A.V. Gerasimov, H. Iacovides, and B.E. Launder. Progress in the generalization of wall-function treatments. *International Journal of Heat and Fluid Flows*, 23:148–160, 2002.

[9] M.H. Hosni, H.W. Coleman, J.W. Gardner, and R.P. Taylor. Roughness element shape effects on heat transfer and skin friction in rough-wall turbulent boundary layer. *International Journal of Heat and Mass Transfer*, 36(1):147–153, 1993.

[10] M.H. Hosni, H.W. Coleman, and R.P. Taylor. Measurements and calculation of surface roughness effects on turbulent flow and heat transfer. Technical Report TFD-89-1, Thermal & Fluid Dynamics Laboratory, Mechanical and Nuclear Engineering Department, Mississippi State University, December 1989.

[11] M.H. Hosni, H.W. Coleman, and R.P. Taylor. Measurements and calculations of rough-wall heat transfer in the turbulent boundary layer. *International Journal of Heat and Mass Transfer*, 34(4/5):1067–1082, 1991.

[12] P.S. Jackson. On the displacement height in the logarithmic velocity profile. *Journal of Fluid Mechanics*, 111:15–25, 1981.

[13] J. Nikuradse. Strömungsgesetze in rauhen Rohren. Technical Report 361, VDI-Forschungsheft, July/August 1933.

[14] J. Nikuradse. Laws of flows in rough pipes. Technical Memorandum 1292, NACA, Washington, April 1937.

[15] A.E. Perry, W.H. Schofield, and P.N. Joubert. Rough wall turbulent boundary layers. *Journal of Fluid Mechanics*, 37:383, 1969.

[16] E. Radenac. Validation of a 3d ice accretion tool on swept wings of the sunset2 program. In *8th AIAA Atmospheric and Space Environments Conference*, number AIAA 2016-3735, Washington, D.C., 2016. AIAA AVIATION Forum.

[17] A. Refloch, B. Courbet, A. Murrone, P. Villedieu, C. Laurent, P. Gilbank, J. Troyes, L. Tessé, G. Chaineray, J.B. Dargaud, E. Quémerais, and F. Vuillot. CEDRE software. *Aerospace Lab*, 2, 2011.

[18] J.A. Robertson. *Surface Resistance as a Function of the Concentration and Size of Roughness Elements*. PhD thesis, State University of Iowa, August 1961.

[19] H. Schlichting. Experimentelle Untersuchungen zum Rauhigkeitsproblem. *Ingenieur Archiv*, VII(1):1–34, February 1936.

DOI: 10.13009/EUCASS2017-372

[20] H. Schlichting. Experimental investigation of the problem of surface roughness. Technical Memorandum 823, NACA, Washington, April 1937.

[21] K. Suga, T.J. Craft, and H. Iacovides. An analytical wall-function for turbulent flows and heat transfer over rough walls. *International Journal of Heat and Fluid Flows*, 27(5):852–866, October 2006.

[22] D.R. Waigh and R.J. Kind. Improved aerodynamic characterization of regular three-dimensional roughness. *AIAA Journal*, 36(6):1117–1119, June 1998.